Available online at www.sciencedirect.com
SCIENCE DIRECT®
Journal of the European Ceramic Society 25 (2005) 3213–3221
www.elsevier.com/locate/jeurceramsoc

PZT phase diagram determination by measurement of elastic moduli

A. Bouzid*, E.M. Bourim, M. Gabbay, G. Fantozzi

Groupe d'Etudes de Métallurgie Physique et Physique des Matériaux (UMR, CNRS 5510), 20 Av. A. Einstein, Bât B. Pascal, 69100 Villeurbanne Cedex, France

Received 2 May 2003; received in revised form 18 May 2004; accepted 4 July 2004
Available online 17 September 2004

Abstract

The aim of the present paper is to investigate the PZT phase diagram and to examine the phase transitions occurring in the low temperature range near the morphotropic phase boundary by using measurement of elastic moduli. The phase transitions are also studied by XRD measurements as a function of temperature. XRD patterns as a function of temperature let us to follow the evolution of lattice parameters and so the determination of phase transitions. Phase transitions identified by Young's and shear modulus anomalies M_1 and M_2 are in accordance with those found by XRD studies and correspond, respectively to the Curie transition—between cubic paraelectric phase and tetragonal ferroelectric phase—and to the morphotropic transition—between both ferroelectric tetragonal and rhombohedral phases or from tetragonal to monoclinic phase. Finally a revisited version of PZT phase diagram is proposed.

Keywords: PZT ceramics; Young's modulus; Shear modulus; Mechanical losses; Phase diagram; X-ray methods

1. Introduction

Lead titanate zirconate $Pb(Zr_{1-x}\ Ti_x)O_3$ ceramics are one of the most used industrial piezoelectric materials, used as transducers, such as phonograph pickups, air transducers, underwater sound and ultrasonic generators, delay line transducers, wave filters etc.[1] All those applications need generally high piezoelectric constants and low dielectric and mechanical losses in the ceramics. The variation of mechanical losses and elastic modulus as function of temperature and excitation frequency can provide direct information on the energy dissipation and phase transitions in the material. Several authors[2–4] have shown that the mechanical losses in the PZT are not only associated with domain walls motion but also with interaction of point defects with domain walls. The ratio Zr/Ti in $Pb(Zr, Ti)O_3$, the nature and concentrations of dopants, the shaping procedure of green bulk, the sintering temperature and atmosphere are the controlling factors to obtain suitable properties for the application. Such variety of controlling factors and wide applications of the PZT materials always incite continuous researches on these materials.

In the PZT ceramics, optimal dielectric and piezoelectric properties are obtained in a zone called morphotropic phase boundary (MPB).[5,6] The width of this zone is not clearly established and several estimations of this zone are proposed in literature.[7,8]

A well-known phase diagram of PZT is provided by Jaffe et al.[1] However, this phase diagram does not give the results below 0 °C. Recently Noheda et al.[9,10] have reported a tetragonal to monoclinic phase transition below room temperature for $x = 0.50$ and 0.52. Further investigations in the MPB done by Ragini et al.[11] show also the coexistence of monoclinic phase with the tetragonal phase. In the present paper, we study the phase transitions for undoped PZT ceramics with different compositions near the morphotropic phase boundary by the measurements of elastic moduli and mechanical losses from −180 to 500 °C and also by XRD as a function of temperature from room temperature to 500 °C. We will present the preparation procedure, the microstructure of the materials, measurement of Young's modulus, M, and mechanical losses, Q^{-1}, at kilohertz frequencies, measurement

* Corresponding author.
E-mail address: gilbert.fantozzi@insa-lyon.fr (G. Fantozzi).

0955-2219/$ – see front matter © 2004 Elsevier Ltd. All rights reserved.
doi:10.1016/j.jeurceramsoc.2004.07.018

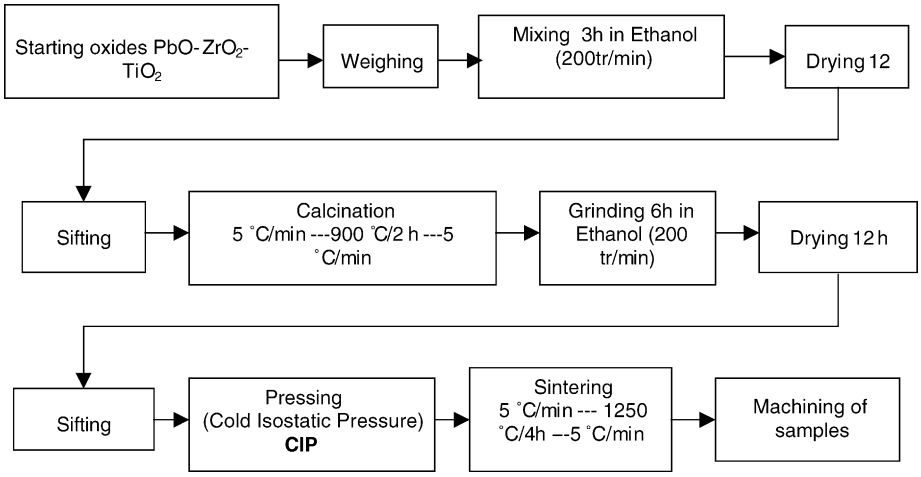

Fig. 1. Processing flow-chart.

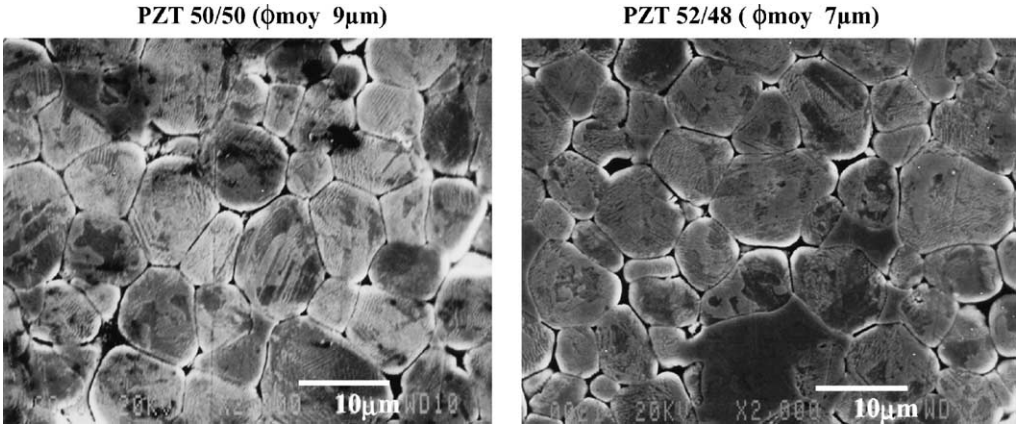

Fig. 2. Microstructure and average grain size (ϕ) of PZT 50/50 and PZT 52/48 materials observed by SEM.

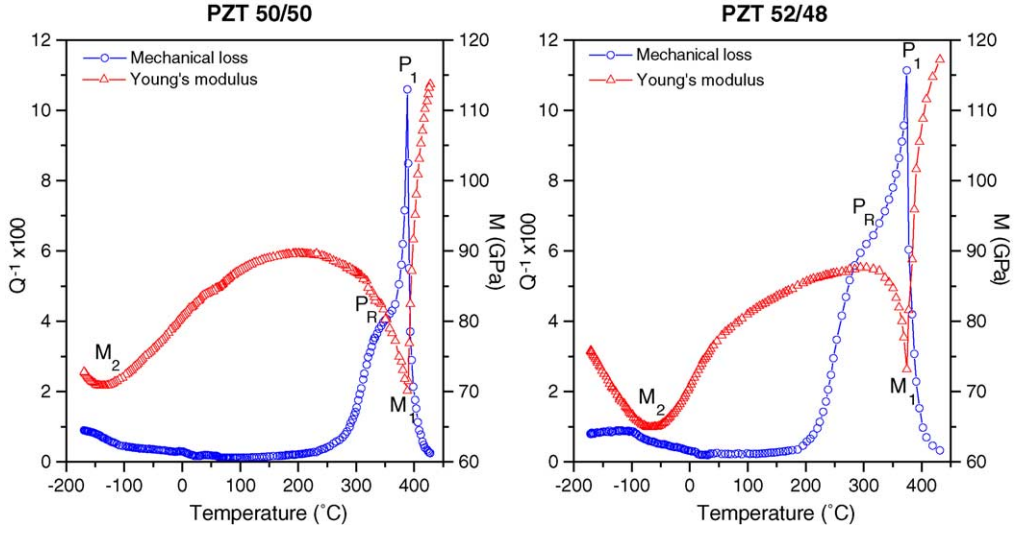

Fig. 3. Mechanical losses $Q^{-1}(T)$ and Young's modulus $M(T)$ for PZT 50/50 and PZT 52/48 materials from −180 to 500 °C.

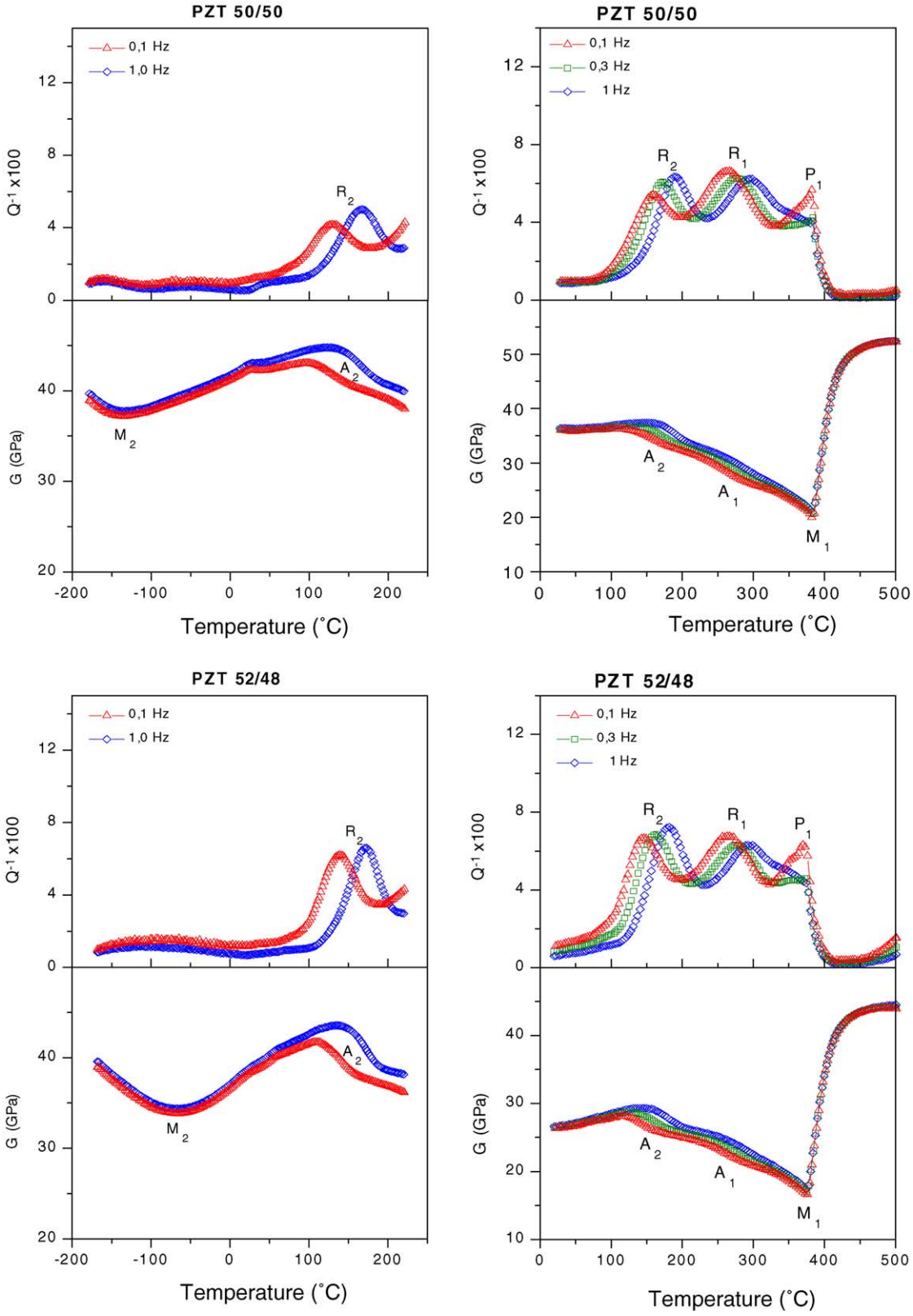

Fig. 4. Mechanical losses $Q^{-1}(T)$ and shear modulus $G(T)$ for PZT 50/50 and PZT 52/48 materials from −180 to 500 °C.

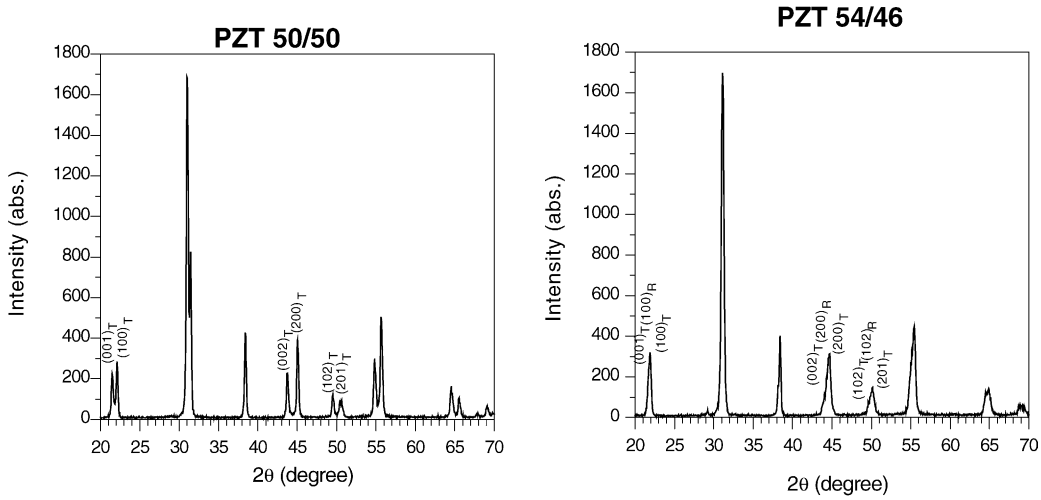

Fig. 5. XRD spectra for PZT 50/50 and PZT 54/46 sintered samples.

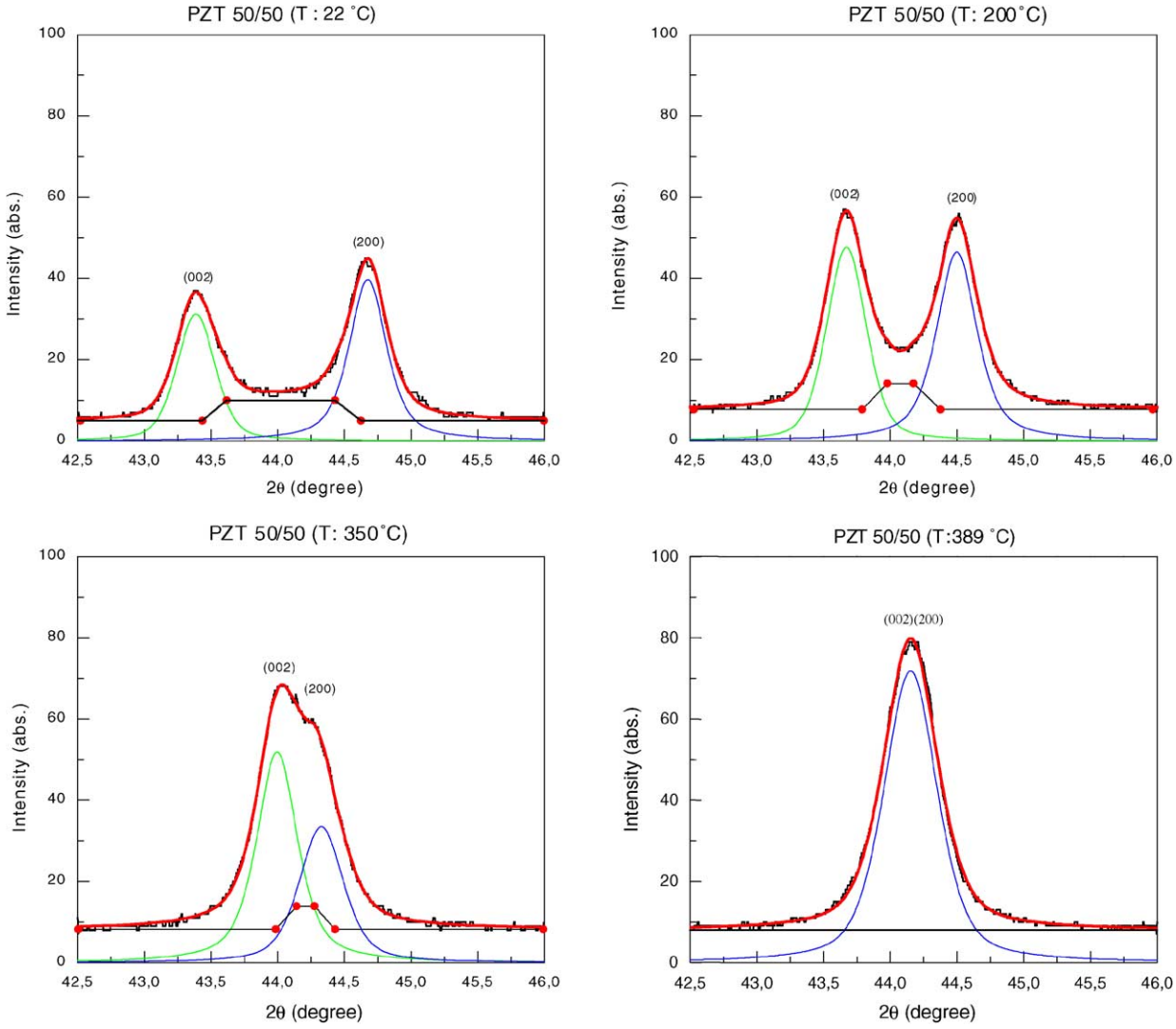

Fig. 6. XRD profiles evolution at different temperatures for PZT 50/50.

of shear modulus, G, and mechanical losses, Q^{-1}, in the hertz frequency range, XRD patterns as a function of temperature and finally an enlarged phase diagram of the PZT ceramics from −180 to 500 °C.

2. Materials and experimental details

The materials used are undoped PZT ceramics prepared by solid state reaction method with the following Zr/Ti ratio: $Pb(Zr_{0.5}Ti_{0.5})O_3$, $Pb(Zr_{0.52}Ti_{0.48})O_3$, $Pb(Zr_{0.54}Ti_{0.46})O_3$, $Pb(Zr_{0.56}Ti_{0.44})O_3$, hereafter shortly labelled as PZT 50/50, PZT 52/48, PZT 54/46 and PZT 56/44.

The procedure of preparation of PZT ceramics is shown by a flow-chart in Fig. 1. The starting powders of PbO, ZrO_2 and TiO_2 were mixed in a planetary grinding mill for 3 h in an agate container with agate balls as grinding media and ethanol as a lubricant. After mixing, the powder was dried overnight at 100 °C in an oven and crushed to pass through a set of sieves of 200 and 100 μm screen. The mixed oxides were calcined in air at 900 °C for 2 h with a heating and a cooling rate of 5 °C/min. The calcined mixture was crushed with the planetary grinding mill for 6 h with ethanol, and then dried overnight at 100 °C in an oven and sifted through 200, 100 and 50 μm screen to eliminate agglomerates. Calcined powder was isostatically pressed at 400 MPa in a plastic bag. The green body was sintered at 1250 °C for 4 h with heating and cooling rate of 5 °C/min. In order to avoid evaporation of PbO and to have equilibrium of stoechiometry of the ceramic after sintering, the ceramic was covered with $PbZrO_3$ packing powder.[12]

Density of the sintered materials was determined by the water displacement method. The sintered samples were examined using a scanning electron microscope (SEM) observation to analyse the microstructure, i.e. shape and size of pores, grains, and ferroelectric domains. These samples were mechanically polished by SiC paper and then lapped by diamond paste of 30, 6, 3, 1 μm. Before observation, the samples were chemically etched by HF solution 5 vol.% in distilled water during 30 s. The average grain sizes were estimated by the line intersection method.

The mechanical loss, Q^{-1}, and Young's modulus, M, as a function of temperature have been measured at kilohertz frequencies.[13] The sample was supported horizontally at its nodal points by two pairs of fine nickel wires. The sample was driven electrostatically in transversal flexural vibration by the application of an amplified sinusoidal tension accompanied by a continual tension. The single excitation-detection electrode was coupled to a conventional frequency modulation (FM) detection system. At each temperature, the resonance curve of the vibration amplitude was recorded, and the internal friction (Q^{-1}) was calculated from:[14]

$$Q^{-1} = \frac{\Delta f}{\sqrt{3} f_r}$$

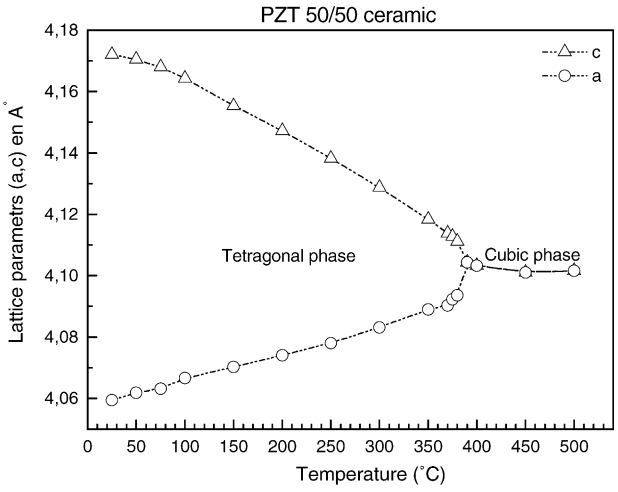

Fig. 7. Lattice parameters variations as function of temperature in PZT 50/50.

where Δf is the resonance curve width at half-height and f_r is the resonance frequency. Young's modulus (E) was calculated from:[15]

$$E = \frac{0.9464 \rho L^4 f_r^2}{d^2}$$

where ρ is the density of sample; L is the length and d is the thickness.

The $Q^{-1}(T)$ and $E(T)$ were measured in vacuum, with a heating rate of 1 °C/min, at a frequency of about 3 kHz, with a maximum strain amplitude of about 10^{-6}.

The mechanical losses, Q^{-1}, and associated shear modulus, G, versus temperature were measured in the Hz frequency range, respectively, at 1, 0.3, 0.1 Hz by using a torsion inverted pendulum, under vacuum, between −180 and 500 °C, at a heating rate of 1 °C/min.

The samples for both medium and low frequencies experiments were rectangular bars with dimensions of 40 mm × 5 mm × 1 mm.

In order to identify the present crystalline phases in sintered materials and to follow the evolution of crystalline structure as a function of temperature, X-ray diffraction (XRD) was performed on Rigaku diffractometer with graphite monochromator [0 0 0 2] by using Cu $K\alpha_1$ radiation. The voltage of X-ray tube was 40 kV, and the current was 25 mA. The compositions of the PZT phases were identified by an analysis of the lines [h 0 0] and [h 0 1] groups, which are split into two peaks in the tetragonal structure (T), and one peak in the rhombohedral structure (R). That gives altogether three peaks containing both structures.

Table 1
Phase transitions temperatures

Compositions	$T_{(C-T)}$ (M_1) (°C)	$T_{(T-R)}$ (M_2) (°C)
PZT 50/50	389 ± 2	−139 ± 3
PZT 52/48	375 ± 2	−69 ± 3
PZT 54/46	371 ± 2	162 ± 3
PZT 56/44	369 ± 2	309 ± 3

The relative densities of the different PZT ceramics were about 93–94%.

Fig. 2 illustrates the microstructures of two PZT ceramics (PZT 50/50, PZT 52/48). The average grain sizes are estimated to be 9, 7, 5, 4 μm for the PZT 50/50, PZT 52/48, PZT 54/46, and PZT 56/44, respectively.

3. Young's modulus *M*, shear modulus *G* and mechanical losses Q^{-1} at kilohertz and hertz frequency range

Fig. 3 shows the variations of mechanical losses, Q^{-1}, and Young's modulus, *M*, as a function of temperature for the PZT 50/50 and PZT 52/48 ceramics. Young's modulus, *M*(*T*), shows two anomalies M_1 and M_2 for all the three compositions. The first anomaly M_1 corresponds to a very sharp peak P_1 on the mechanical losses curves. However, there is no peak on the mechanical losses curves corresponding to the second anomaly M_2. The temperatures of these anomalies are dependent on the composition of materials.

Fig. 4 shows the variations of mechanical losses, Q^{-1}, and shear modulus, *G*, as a function of temperature for the PZT 50/50 and PZT 52/48 ceramics. Shear modulus, *G*(*T*), shows also two anomalies M_1 and M_2 for both compositions. From the anomalies temperatures and according to the phase transition diagram, the M_1 associated with the me-

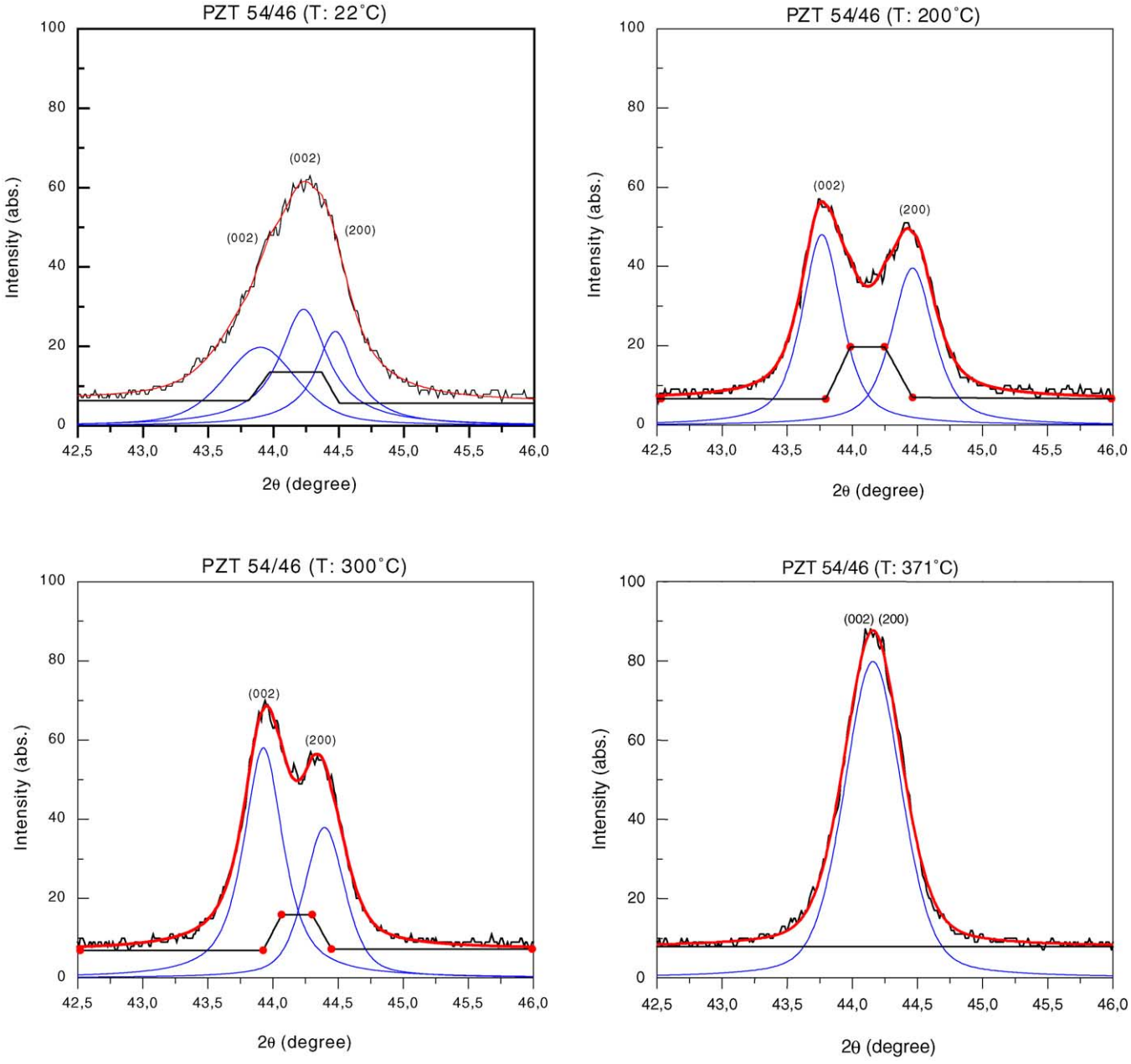

Fig. 8. XRD profiles evolution at different temperatures for PZT 54/46.

chanical losses P_1 peak is attributed to the transition between cubic and tetragonal.[16] However the M_2 could be attributed to the transition from tetragonal to rhombohedral[16] or to the transition between tetragonal and monoclinic phases.

The monoclinic structure can be considered as a bridge between the rhombohedral and tetragonal phases in the region of the MPB.[9–11] The phase transitions temperatures obtained from the M_1 and M_2 temperatures are given in Table 1.

4. XRD phase studies

Fig. 5 shows the XRD patterns of the sintered samples for PZT 50/50 and PZT 54/46 compositions. X-ray scans were carried out at room temperature with a step of 0.05° and a scanning speed of 2°/min from 2θ equal 20°–70°. The composition PZT 50/50 showed one set of peaks corresponding to tetragonal ferroelectric phase as expected from the phase-equilibrium diagram. The diffraction lines which were split into triplets for the composition PZT 54/46, indicated the coexistence of both tetragonal and rhombohedral ferroelectric phases.[17–19]

To follow the evolution of crystalline structure of sintered samples as a function of temperature and estimate the lattice parameters, we have analysed the peaks [$(0\,0\,2)_T$, $(2\,0\,0)_R$, $(2\,0\,0)_T$] in the 2θ range 42.5°–46° because their intensity is enough large to perform good measurements. In order to ensure an accurate determination of lattice parameters of units cells, the X-ray scans were recorded with a step of 0.002° and scanning speed of 0.025°/min. The data obtained were fitted with the sum of several Lorenzian lines using a computer and adjusted with a plateau attributed to the contribution of ferroelectric domain walls in diffraction.[20] Thus the required informations such as the number of lines, their angular positions and their relative intensities are obtained. The lattice parameters a_T and c_T of tetragonal structure were calculated from the doublet (2 0 0).

Fig. 6 illustrates the evolution of XRD profiles from 42.5° to 46.0° of 2θ for PZT 50/50 ceramic at different temperatures: 22, 200, 350 and 389 °C. The XRD profiles below 389 °C can be identified as tetragonal ferroelectric phase; the XRD profiles above 389 °C can be identified as cubic paraelectric phase.

Fig. 7 shows the variations of lattice parameters c[0 0 1] and a[1 0 0] in the tetragonal phase and a[1 0 0] in the cubic phase as a function of temperature. The phase transition from tetragonal to cubic phase (T_C) is located near 389 °C.

However, for the PZT 54/46 ceramics, the XRD profile at room temperature is complex (Fig. 8), and cannot be uniquely identified as a tetragonal phase. Such multiplicity of the profiles of XRD could be interpreted as a mixture of tetragonal phase and rhombohedral phase. By using Lorentz function, a decomposition of the diffraction profile lines is performed. When the temperature is above 200 °C, the XRD profiles become simple and can be easily identified as tetragonal phase. When the temperature reaches 371 °C, the crystalline structure becomes cubic. The results of the lattice parameters are shown in Fig. 9. The Curie temperature (T_C) corresponding to phase transition from tetragonal to cubic is located at 371 °C. However, the phase transition from rhombohedral to tetragonal cannot be easily determined by the variation of the lattice parameters because uncertainty of the decomposition of the XRD profiles lines.

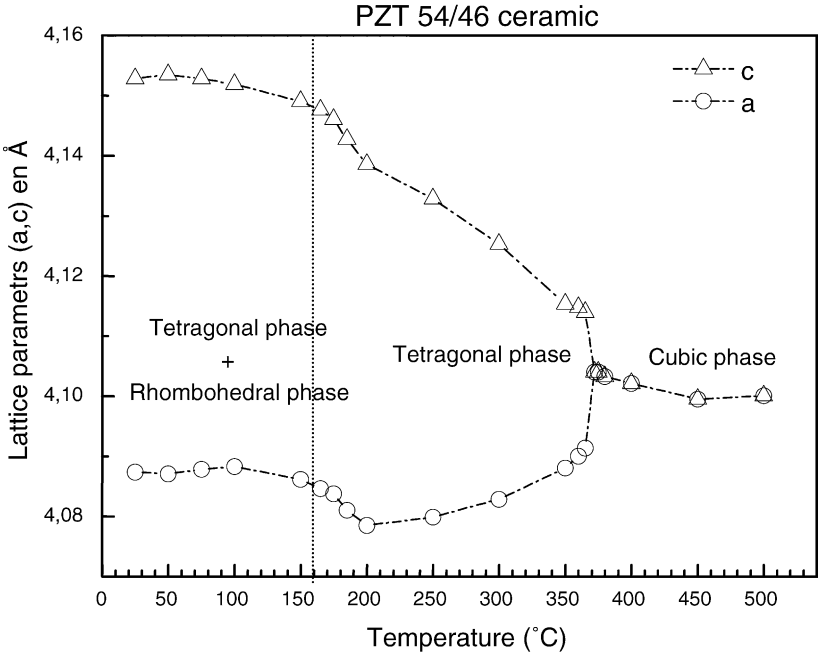

Fig. 9. Lattice parameters variations as function of temperature in PZT 54/46.

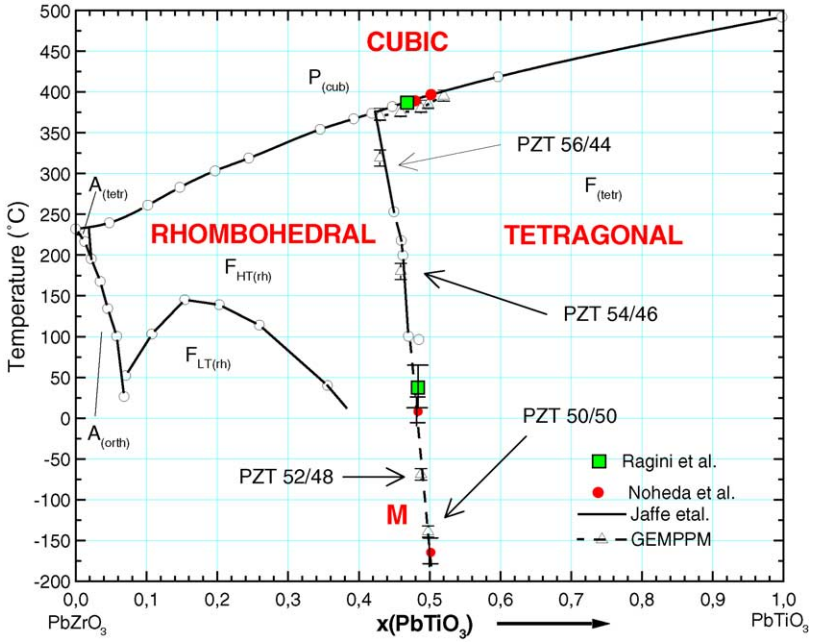

Fig. 10. PZT phase diagram. M for monoclinic phase.

Phase transitions temperatures obtained from XRD measurements are in accordance with those determined by measurements of elastic moduli shown in Table 1.

5. Phase diagram of PZT ceramics

A good accordance is found when reporting our phase transitions temperatures results obtained from the measurement of elastic moduli on the Jaffe et al.[1] diagram, as shown by Fig. 10 for the high temperature part of the diagram. Measurements at low temperatures are also shown in Fig. 10. The recent results obtained by Noheda et al.[9,10] and Ragini et al.[11] are equally indicated. All the results are in agreement but it can be noticed that the measurement of elastic moduli is a suitable, easy and fast method to determine the phase transitions in PZT materials.

6. Conclusion

A series of undoped PZT ceramics with compositions near the morphotropic phase boundary are prepared such as PZT 50/50, PZT 52/48, PZT 54/46 and PZT 56/44. Phase transitions in these materials are studied by Young's modulus and shear modulus with their associated mechanical losses at medium and low frequencies from −180 to 500 °C on one hand and by XRD versus temperature on the other hand. The two anomalies M_1 and M_2 observed on Young's modulus and shear modulus as a function of temperature correspond to the phase transitions from cubic to tetragonal phase and from tetragonal to rhombohedral or from tetragonal to monoclinic phase.[9–11] These two transitions are also confirmed by the evolution of XRD patterns as a function of temperature. Thus, an enlarged phase diagram of PZT ceramics is obtained especially in the low temperature range from the report of our results and those of Noheda et al.[9,10] and Ragini et al.[11] on the Jaffe et al.[1] phase diagram. Finally, It is useful to emphasize that the measurement of elastic moduli provides a suitable method to determine the phase transitions in ceramics.

References

1. Jaffe, B., Cook, W. R. and Jaffe, H., *Piezoelectric Ceramics*. Academic Press, London, 1971, p. 317.
2. Postnikov, V. S., Pavlov, V. S. and Turkov, S. K., Internal friction in ferroelectrics due to interaction of domain boundaries and point defects. *J. Phys. Chem. Solids*, 1970, **31**, 1785–1791.
3. Bourim, E. M., Tanaka, H., Gabbay, M. and Fantozzi, G., Internal friction and dielectric measurements in lead zirconate titanate ferroelectric ceramics. *Jpn. J. Appl. Phys.*, 2000, **39**, 5542–5547.
4. Wang, Can., Fang, Q. F., Shi, Yun. and Zhu, Z. G., Internal friction study on oxygen vacancies and domain walls in Pb(Zr, Ti)O_3. *Mater. Res. Bull.*, 2001, **36**, 2657–2665.
5. Jaffe, B., Roth, R. S. and Marzullo, S., Piezoelectric properties of lead zirconate–lead titanate solid solution ceramic ware. *J. Res. Nat. Bur. Stand*, 1955, **55**(5), 239–254.
6. Soares, M. R., Senos, A. M. R. and Mantas, P. Q., Phase coexistence region and dielectric properties of PZT ceramics. *J. Eur. Ceram. Soc.*, 2000, **20**, 321–334.
7. Babulescu, A., Barbulescu, Eva and Darb, D., Phase transition in PZT solid solutions. *Ferroelectrics*, 1983, **47**, 221–230.
8. Mishra, S. K., Singhi, A. P. and Pandey, D., Thermodynamic nature of phase transitions in $Pb(Zr_xTi_{1-x})O_3$ ceramics near the morphotrpic phase boundary. II. Dielectric and piezoelectric studies. *Philos. Mag.*, 1997, **76**(2), 213–226.

9. Noheda, B., Cox, D. E., Shirane, G., Gonzalo, J. A., Cross, L. E. and Park, S.-E., A monoclinic ferroelectric phase in the $Pb(Zr_{1-x}Ti_x)O_3$ solid solution. *Appl. Phys. Lett.*, 1999, **74**(14), 2059–2061.
10. Noheda, B., Gonzalo, J. A., Cross, L. E., Guo, R., Park, S.-E., Cox, D. E. *et al.*, Tetragonal-to-monoclinic phase transition in a ferroelectric perovskite: the structure of $Pb(Zr_{0.52}Ti_{0.48})O_3$. *Phys. Rev. B*, 2000, **61**(13), 8687–8695.
11. Ragini, Rajeev Ranjan, Mishra, S. K. and Pandey, D., Room temperatre structure of $Pb(Zr_xTi_{1-x})O_3$ around the morphotropic phase boundary region: a Rietveld study. *J. Appl. Phys.*, 2002, **92**(6), 3266–3274.
12. Kingon, A. I. and Clark, J. B., Sintering of PZT ceramics. I. Atmosphere controlling. *J. Am. Ceram. Soc.*, 1983, **66**(4), 253–260.
13. Cheng, B. L., Gabbay, M., Duffy Jr., W. and Fantozzi, G. J., *Alloys Compd.*, 1994, **211/212**, 344–347.
14. Zener, C., *Elasticity and Anelasticity of Metals*. University of Chicago Press, Chicago, IL, 1948, p. 60.
15. Nowick, A. S. and Berry, B., *Anelastic Relaxation in Crystalline Solids*. Academic Press, New York, NY, 1972, pp. 627–629.
16. Bourim, E. M., Idrissi, M. H., Cheng, B. L., Gabbay, M. and Fantozzi, G., Elastic modulus and mechanical loss associated with phase transitions and domain walls motions in PZT based ceramics. *J. Phys. IV*, 1996, **6**(C8), 633–636.
17. Boutarfaia, A. and Bouaoud, E., Tetragonal and rhombohedral phase co-existence in the system: $PbZrO_3$–$PbTiO_3$–$Pb(Fe_{1/5}, Ni_{1/5}, Sb_{3/5})O_3$. *Ceram. Int.*, 1995, **22**, 281–286.
18. Soares, M. R., Senos, A. M. R. and Mantas, P. Q., Phase coexistence in PZT ceramics. *J. Eur. Ceram. Soc.*, 1999, **19**, 1865–1871.
19. Boutarfaia, A., Boudaren, S. E., Mousser, A. and Bouaoud, E., Study of phase transition line of PZT ceramics by X-ray diffraction. *Ceram. Int.*, 1995, **21**, 391–394.
20. Valot, C. M., Floquet, N., Perriat, P., Mesnier, M. and Niepce, J. C., Ferroelectric domains in $BaTiO_3$ powders and ceramics evidenced by X-ray diffraction. *Ferroelectrics*, 1995, **172**, 235–241.